



Ag/Cd coordination architecture and photoluminescence behaviors

Jiyong Hu^a, Yujie Zhao^a, Fan Yang^a, Chunli Liao^b and Jin'an Zhao^a

^aCollege of Material and Chemical Engineering, Henan University of Urban Construction, Pingdingshan, PR China; ^bCollege of Life Science and Engineering, Henan University of Urban Construction, Pingdingshan, PR China

ABSTRACT

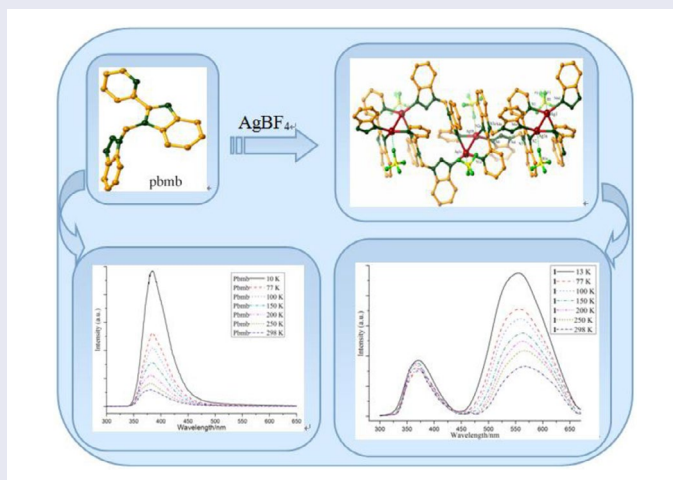
Three coordination architectures, {[Ag₄(pbmb)₄·(BF₄)₄](CH₃OH)₂·H₂O}_n (**1**), {[Cd₂(pbmb)₄](ClO₄)₄·(CH₃OH)₅}_n (**2**), and [Cd₄(pbmb)₄·1₈(CH₃OH)₂]_n (**3**) (pbmb = 1-((2-(pyridin-2-yl)-1H-benzoimidazol-1-yl)methyl)-1H-benzotriazole), are built up from Ag(I)/Cd(II) salts and a flexible pyridyl-benzimidazole-based organic spacer. Single-crystal analysis shows that **1** and **2** have 1-D chains, while **3** displays a tetranuclear structure. All complexes exhibit different coordination geometries and properties, which can be attributed to the difference between the metal centers or anions. In the case of **1** in particular, the Ag···Ag interactions play a crucial role in the formation of a supramolecular architecture. The binuclear-based complex consists of a pair of Ag···Ag contacts (*ca.* 2.953 Å), and it exhibits intense triplet emission with large Stokes shift and high thermal stability. Compared to pbmb, **2** has excellent high-energy fluorescence properties, while **1** and **3** exhibit mainly low-energy emission. Therefore, it can be concluded that the heavy atom effect has a causative influence in enhancing the triplet state radiative rate, resulting in large Stokes' shift of the complex.

ARTICLE HISTORY


Received 3 August 2017
Accepted 17 March 2018

KEYWORDS

Ag complex; argentophilic contact; large Stokes shift; photoluminescence behavior



CONTACT Jiyong Hu ✉ hujiyong@hncj.edu.cn; Jin'an Zhao ✉ zjinan@zzu.edu.cn

 The supplemental data for this article can be available at <https://doi.org/10.1080/00958972.2018.1467008>.

1. Introduction

Attention has been directed toward the design and development of precise functional devices in the nanometer and sub-nanometer scale [1–3]. An interesting synthetic strategy involves coordination-driven, self-assembly harnessing of the directionality of metal–ligand interactions and the structural versatility of metal centers. The objective is to promote the development of elegant architectures with unusual behaviors and ingenious applications at the molecular level [4, 5]. These structural and electronic properties can be optimized by variation of building blocks, *i.e.* the metal has a more or less preferred coordination environment. In addition, the organic synthons provide donors in the specific positions for coordination, and potential interaction sites to generate noncovalent secondary interactions, such as hydrogen bonding and $\pi \cdots \pi$ stacking [6, 7]. Such contacts may be important for properties such as molecular recognition, catalysis, *etc.* However, although remarkable progress has been made in the synthesis and study of metal complexes, the formation of supramolecular architectures is still a challenging issue, due to various impact factors such as metal-to-ligand ratio, the nature of the metal center and ligand, anions, solvent, pH of the reaction, temperature, *etc.* [8, 9]. Anions play crucial roles; anion with larger size and hydrogen bonding interactions will significantly affect the constructions and properties of the compounds [10, 11].

To achieve desired architectures with useful functions, a variety of metal centers have been used to react with organic linkers. Different metal centers tend to result in different structures and functions of the coordination compounds. For example, Zhu's group reported several electrochemically active complexes, in which the metal centers played an important role in the improvement of photocurrent response [12]. The study of metal–organic compounds has attracted interest because of their interesting structures and promising potential. Ag(I)-containing compounds are of particular interest due to their unusual functions and potential properties. The d^{10} closed-shell electronic configuration of Ag(I) imposes few structural requirements on the surrounding ligands and anion entities. Despite the repulsion expected between two closed-shell metal centers, Ag(I) coordination compounds with short $\text{Ag} \cdots \text{Ag}$ contacts, from dimers to intricate high-nuclear clusters, have been characterized [13–16]. These metal aggregates consisting of such short $\text{Ag} \cdots \text{Ag}$ interactions have attracted interest and are the origin of a wide variety of fascinating behaviors. Among the aggregates, a rich photophysical property may be anticipated because of the presence of $\text{Ag} \cdots \text{Ag}$ contacts, which could play a pivotal role in governing the emission characteristics of luminescent Ag complexes. Although silver and cadmium are d^{10} transition metals, their coordination patterns are very different. Cadmium generally does not form Cd–Cd bonds and its coordination flexibility is inferior to silver [17–20]. In this article, three new Cd and Ag coordination compounds based on the ligand pbmb, $\{[\text{Ag}_4(\text{pbmb})_4 \cdot (\text{BF}_4)_4](\text{CH}_3\text{OH})_2 \cdot \text{H}_2\text{O}\}_n$ (**1**), $\{[\text{Cd}_2(\text{pbmb})_4](\text{ClO}_4)_4 \cdot (\text{CH}_3\text{OH})_5\}_n$ (**2**), and $[\text{Cd}_4(\text{pbmb})_4 \cdot \text{I}_8(\text{CH}_3\text{OH})_2]_n$ (**3**), were synthesized. Their luminescence properties were also studied, and the results indicate that the characteristic feature of the compounds can be affected by the metal centers, anions, and coordination environments. A ligand supported Ag complex **1** with argentophilic attraction and two structurally different Cd complexes **2** and **3** based on different anions have been synthesized. Complex **2** has excellent high-energy fluorescence, whereas **1** and **3** exhibited mainly low-energy band emission due to the Ag and I[−] heavy atom effect.

2. Experimental

2.1. Materials and general methods

All the starting materials were purchased commercially as reagent grade and used without purification. 1-((2-(Pyridin-2-yl)-1H-benzimidazol-1-yl)methyl)-1H-benzotriazole (pbmb) was synthesized according to a literature method [21]. The thermogravimetric experiments were performed using a NETZSCH STA 449F3 instrument (heating rate at 10 °C/min). FT-IR spectra were recorded on a Frontier spectrophotometer (Perkin Elmer, U.S.A.) with KBr pellets from 400–4000 cm⁻¹. Elemental analyses (C, H, and N) were carried out with a Flash EA 1112 elemental analyzer. The luminescence and corresponding lifetime measurements of **1** were established by Edinburgh Analytical Instruments FLS920 at 10, 77, 100, 150, 200, 250, and 298 K in solid state. The emission spectra of **2** and **3** were performed on a F-4600 fluorescence spectrophotometer (Hitachi).

2.2. Synthesis of {[Ag₄(pbmb)₄·(BF₄)₄](CH₃OH)₂·H₂O}_n (**1**)

A reaction mixture of AgBF₄ (0.03 mmol, 0.0058 g), pbmb (0.02 mmol, 0.0065 g), chloroform (1 mL) and methanol (1 mL) was placed in a glass reactor, and mixture was sealed and heated at 85 °C for three days; then the reaction system was cooled to room temperature. Colorless block crystals of **1** were obtained in 45% yield (based on Ag). Elemental analysis (%): Calcd for (C₇₈H₆₆Ag₄B₄F₁₆N₂₄O₃): C, 43.21; H, 3.07; N, 15.50. Found: C, 43.07; H, 2.88; N, 15.52. IR (KBr/pellet, cm⁻¹): 3321w, 1594w, 1525w, 1451m, 1387m, 1297m, 1191m, 1049s, 747s, 597m.

2.3. Synthesis of {[Cd₂(pbmb)₄](ClO₄)₄·(CH₃OH)₃}_n (**2**)

A solution of pbmb (0.0065 g, 0.02 mmol) in methanol (1 mL) was added dropwise into a solution of Cd(ClO₄)₂·6H₂O (0.0126 g, 0.03 mmol) in methanol (1 mL). The mixed solution was heated at 85 °C for 36 h. Colorless block crystals of **2** suitable for X-ray analysis were collected. Yield: 48% (based on Cd). Elemental analysis (%): Calcd for (C₈₁H₇₆Cd₂Cl₄N₂₄O₂₁): C, 46.59; H, 3.67; N, 16.10. Found: C, 46.12; H, 3.24; N, 16.45. IR (KBr/pellet, cm⁻¹): 3429w, 3072w, 1602m, 1594m, 1480m, 1457m, 1431s, 1402m, 1337w, 1158m, 1090s, 1005m, 790m, 744s, 623s.

2.4. Synthesis of [Cd₄(pbmb)₄·I₈(CH₃OH)₂]_n (**3**)

A solution of pbmb (0.0065 g, 0.02 mmol) in methanol (4 mL) was added dropwise into a solution of CdI₂ (0.0110 g, 0.03 mmol) in chloroform (1 mL). The mixture was left to stand at room temperature for slow evaporation for a week. Clusters of yellow brown crystals of **3** suitable for X-ray analysis were collected. Yield: 56% (based on Cd). Elemental analysis (%): Calcd for (C₇₈H₆₄Cd₄I₈N₂₄O₂): C, 33.05; H, 2.28; N, 11.86. Found: C, 33.41; H, 2.60; N, 11.68. IR (KBr/pellet, cm⁻¹): 3201w, 3048w, 1597 m, 1478 m, 1450s, 1435s, 1380 m, 1300 m, 1268 m, 1192w, 1108w, 1004w, 977w, 791 m, 745s, 694w, 632w.

Table 1. Crystal data and structure refinement for **1–3**.

Complex	1	2	3
Formula	C ₇₈ H ₆₆ Ag ₄ B ₄ F ₁₆ N ₂₄ O ₃	C ₈₁ H ₇₆ Cd ₂ Cl ₄ N ₂₄ O ₂₁	C ₇₈ H ₆₄ Cd ₄ N ₂₄ O ₂
fw	2166.26	2088.25	2834.33
Temp (K)	100(10)	100.01(10)	150.01(10)
λ (Cu Kα), Å	1.5418	1.5418	0.71073
Crystal system	Monoclinic	Monoclinic	Triclinic
Space group	C2/c	P2 ₁ /n	P-1
a (Å)	17.8850(1)	15.7842(3)	10.7037(3)
b (Å)	13.1636(7)	16.1543(3)	11.2516(4)
c (Å)	18.2682(9)	16.9425(3)	19.2097(6)
α (deg)	90.00	90	83.556(3)
β (deg)	98.806(5)	90.1258(15)	75.282(3)
γ (deg)	90.00	90	76.009(3)
V (Å ³)	4250.2(4)	4320.02(13)	2168.00(13)
Z	2	4	1
θ _{max} (deg)	4.188–70.074	3.781–70.07	2.86–27.10
F(000)	2156	2124.0	1332.0
Final R1 ^a , wR2 ^b	0.0665, 0.1709	0.0689, 0.1986	0.0341, 0.0668
Goodness-of-fit on F ²	1.108	1.057	1.041

$$^aR1 = \sum ||F_o| - |F_c|| / \sum |F_o|$$

$$^bwR2 = [\sum w(|F_o|^2 - |F_c|^2)|^2 / \sum w|F_o|^2]^{1/2}$$

2.5. Crystal structure determination

A crystal suitable for X-ray determination was mounted on a glass fiber. The data were collected on a SuperNova diffractometer with graphite monochromated Cu-Kα radiation (λ = 1.54184 Å) at 100(2) K for **1** and **2**, whereas **3** was collected with Mo-Kα radiation (λ = 0.71073 Å) at 150.01(10) K. The structures were solved by direct methods and expanded with Fourier techniques. The non-hydrogen atoms were refined anisotropically. Hydrogens were included but not refined. The final cycle of full-matrix least-squares refinement was based on observed reflections and variable parameters. Using OLEX2, the structure was solved with the superflip structure solution program using Charge Flipping and refined with the SHELXL refinement package using least squares minimization [22–25, 26]. Table 1 shows crystal data and processing parameters for **1–3** and Table 2 lists selected bond lengths and angles.

3. Results and discussion

3.1. Crystal structure of {[Ag₄(pbmb)₄·(BF₄)₄](CH₃OH)₂·H₂O}_n (**1**)

The structure of **1** is depicted in Figure 1. The fundamental unit consists of one pbmb synthon, one Ag(I) center, one quarter aqua molecule, half a methanol and one BF₄⁻, with a BF₄⁻ and free solvent molecules balancing the charge and stabilizing the structure. The short Ag(I)⋯Ag(I) separation (2.953 Å) between the adjacent intrachain Ag(I) centers is shorter than the sum of the van der Waals radii for Ag (3.4 Å) and very close to the Ag⋯Ag separation in silver metal (2.89 Å). This suggests the presence of Ag(I)⋯Ag(I) ligand supported interactions [27–29]. Based on such argentophilic attraction, two adjacent Ag(I) centers are double bridged to form a dimeric moiety. Among the reported metal center contacts, two outstanding strategies have been employed for the self-assembly process. One is that the O²⁻, OH⁻, and the utilized halide may play crucial roles in forming clusters with μ₂, μ₃, and μ₄ bridging modes. The other is the combination of the multidentate connector with metal centers for

Table 2. Selected bond lengths and angles for **1–3**.

Complex 1			
Ag1–N2 ^{#1}	2.297(5)	Ag1–N1	2.248(6)
Ag1–N6 ^{#2}	2.313(5)	N2 ^{#1} –Ag1–N6 ^{#2}	92.32(2)
N1–Ag1–N2 ^{#1}	131.2(19)	N1–Ag1–N6 ^{#2}	135.4(2)
Complex 2			
Cd1–N1	2.370(4)	Cd1–N7	2.364(4)
Cd1–N2	2.350(4)	Cd1–N8	2.358(4)
N6–Cd1 ¹	2.334(4)	N6 ¹ –Cd1–N8	169.37(15)
N6 ¹ –Cd1–N7	101.10(15)	N8–Cd1–N1	103.04(14)
N8–Cd1–N7	71.36(14)	N2–Cd1–N8	79.57(16)
N2–Cd1–N1	71.78(14)	N2–Cd1–N7	105.04(14)
Complex 3			
I4–Cd2	2.7719(4)	I2–Cd1	3.0032(4)
I2–Cd2	2.8592(4)	Cd1–N7	2.401(4)
Cd1–N2	2.354(3)	Cd1–N1	2.392(3)
Cd2–I3	2.7226(5)	N7–Cd1–I2	82.88(8)
N7–Cd1–I1	99.97(8)	N2–Cd1–I2	163.26(8)
N2–Cd1–N1	71.11(11)	I3–Cd2–I4	117.283(15)

Symmetry transformation used to generate equivalent atoms: #1 $1 - X, +Y, 1/2 - Z$; #2 $+X, 2 - Y, -1/2 + Z$ for **1**. #1 $1 - X, 2 - Y, 1 - Z$ for **2**.

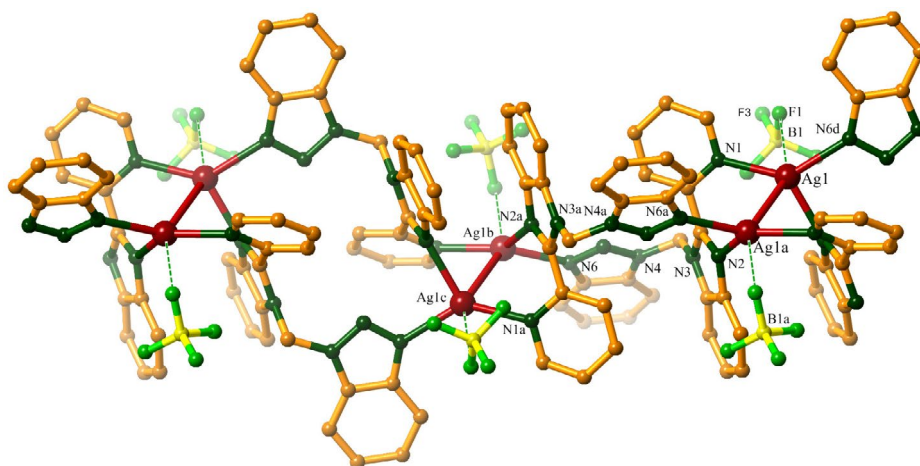


Figure 1. A view of the Ag(I) center with partial atom numbering schemes of **1**; the hydrogens and uncoordinated solvent molecule are omitted for clarity.

constructing clusters. The N-containing connectors, such as the pyridine, triazole, tetrazole, and their derivatives, are frequently used to generate products [30]. Herein, to gain an in-depth understanding of the nature of the pyridyl-benzimidazole system, the organic connector ((2-(pyridin-2-yl)-1H-benzimidazol-1-yl)methyl)-1H-benzotriazole was selected. Furthermore, within the dimeric moiety of **1**, separation between two centroids of the benzene ring from the benzimidazole segment is 3.622 Å with a dihedral angle of 7°. In this case, such $\pi \cdots \pi$ interaction will reinforce argentophilic interaction (Figure S1). The four-coordinate Ag(I) center can be regarded as a distorted trigonal-pyramid, in which the equatorial positions are occupied by three nitrogens from pyridyl, benzimidazole, and benzotriazole

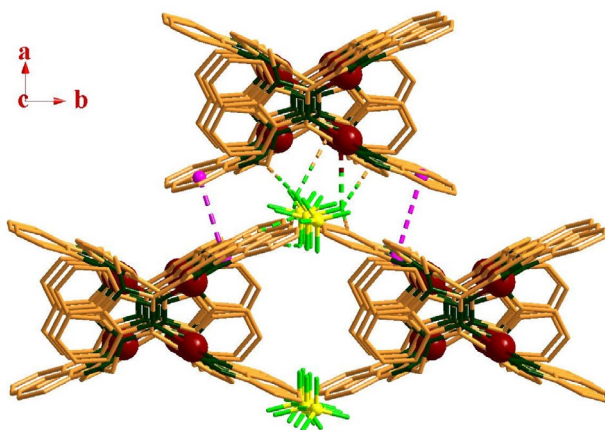


Figure 2. The $\pi\cdots\pi$ and $C\cdots F$ interactions extended the 1-D chains in both a and b -axis directions.

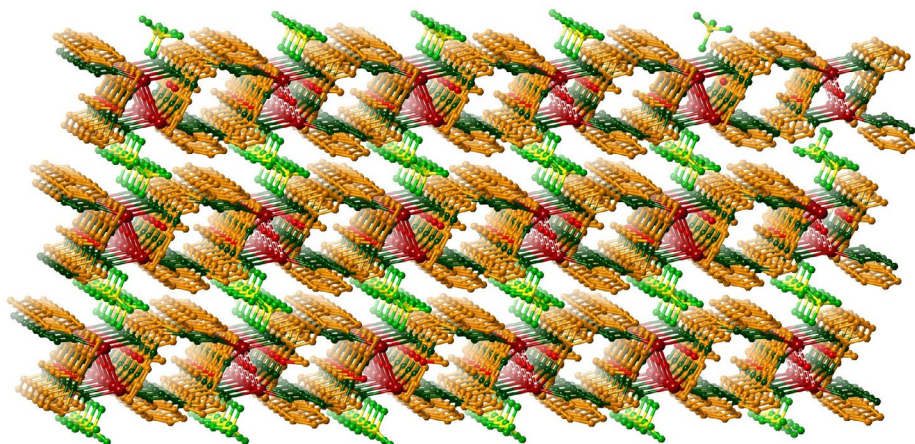


Figure 3. Packing of the repeating 1-D chains in the structure of **1**. For clarity the hydrogens and solvents are not shown.

segments of three pbmb synthons. In addition, the axial site is occupied by one fluoride with the angle O2–Ag1–F1 of 116.044°.

Each dimeric moiety links equivalent ones via double pbmb connectors to produce a 1-D chain along the c -axis. The anion BF_4^- is often noncoordinating, but in this case, there are weak interactions between fluorine and Ag(I) atoms ($Ag(I)\cdots F = 3.132 \text{ \AA}$), and their separation distance is shorter than their corresponding van der Waals contact of 3.19 \AA [31]. The closest separation of the benzene ring and triazole ring from benzotriazole segments is 3.764 \AA , with a dihedral angle of 0.7° , which indicates the presence of $\pi\cdots\pi$ interactions between the adjacent chains (Figure 2). The extended adjacent 1-D chains along both a and b axes due to $\pi\cdots\pi$ and $C\cdots F$ interactions are 3.229 \AA for $C2\cdots F2$, 2.959 \AA for $C13\cdots F4$, 3.198 \AA for $C15\cdots F1$, 3.119 \AA for $C16\cdots F2$ and 3.190 \AA for $C18\cdots F3$. These values are in the range of reported $C\cdots F$ interactions [32], in forming a 3-D network (Figure 3).

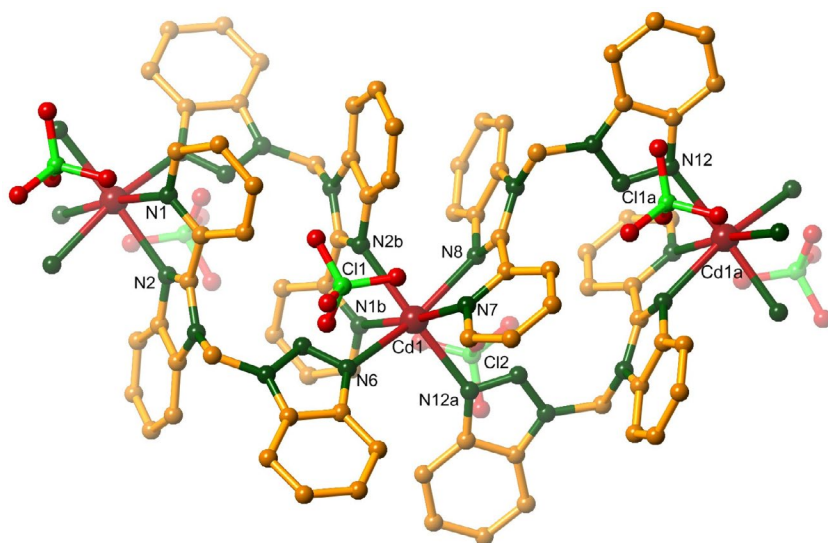


Figure 4. The coordination environments of Cd(II) in **2**.

3.2. Crystal structure of $\{[Cd_2(pbmb)_4](ClO_4)_4 \cdot (CH_3OH)_5\}_n$ (**2**)

We chose cadmium salts containing different anions (ClO_4^- and I^-) to react with a free ligand, resulting in structurally different **2** and **3**. Single-crystal X-ray diffraction analyses revealed that **2** crystallizes in a monoclinic $P 2_1/n$ space group with a 1-D coordination framework. The asymmetric unit of **2** is composed of one Cd(II), two pbmb, two and a half methanol molecules and two ClO_4^- anions, as depicted in Figure 4. The six-coordinate Cd(II) center is defined by six nitrogens from four pbmb ligands, with two nitrogens (N12a, N2b) at the apical positions and the others (N1b, N6, N7, N8) positioned at the equatorial plane to produce a regular octahedral coordination geometry. The Cd–N distances are from 2.334 Å to 2.370 Å, within the normal range compared with other Cd complexes [33, 34]. The Cd(II) centers and the pyridine, benzimidazole, and benzotriazole moieties of the multifunctional pbmb are bridged to form a binuclear metallacycle, where the $Cd \cdots Cd$ ($Cd1 \cdots Cd1a$) has a minimum distance of 8.2537 Å. The binuclear metallacycle is further linked via the pbmb linkers to a 1-D chain structure. Compared with **1**, their structures and coordination patterns vary because of the difference between metal centers, although both BF_4^- and ClO_4^- have tetrahedral geometries. This can be attributed to the difference between the metal centers and indicates that the structures and properties of the compounds can be affected by the metal center.

3.3. Crystal structure of $[Cd_4(pbmb)_4 \cdot I_8(CH_3OH)_2]_n$ (**3**)

In contrast to **2**, changing the anion to I^- resulted in a different supramolecular structure. Single-crystal analysis revealed that **3** has a tetranuclear structure in the triclinic system with space group $P\bar{1}$. The fundamental unit contains two Cd(II) centers, two pbmb synthons, four I^- anions, and one methanol molecule. The Cd1 is six-coordinate in a distorted octahedral geometry, comprised of N6 and N7 in the apical positions and N1a, N2a, I1, and I2 in the

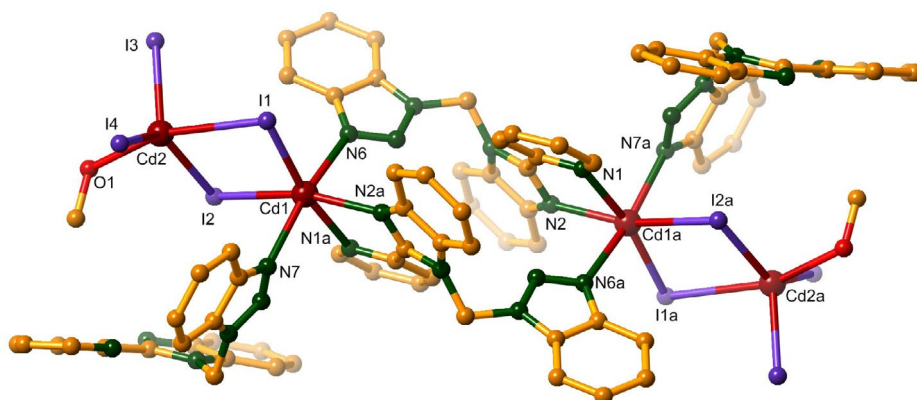


Figure 5. Molecular structure and atom numbering scheme for tetranuclear **3**; hydrogens have been omitted for clarity.

equatorial plane, whereas Cd2 is five-coordinate. The Cd–I bond lengths are 2.723–3.281 Å and the Cd–N distances vary from 2.354 Å to 2.436 Å, which are comparable with other Cd-based compounds [35, 36]. As shown in Figure 5, the two Cd(II) centers form a binuclear unit via two I[−] anions, and the adjacent pairs of the binuclear units are double-bridged by two ligands to form a tetranuclear structure. The 3-D supramolecular stacking structures are shown in Figures S2 and S3. Compared with **2**, they are structurally different due to their different anions, although they are all complexes of cadmium. Thus, the anion plays an important part in the structure of complexes and influences the properties of the resulting compounds. Structurally different Cd(II) complexes have also been investigated by Zheng's group due in part to the different coordination behavior of inorganic anions. They found that the 3-D frameworks induced by anion regulated the different binuclear Cd(II) secondary building units [37].

3.4. Luminescence properties

The air-stable **1** can retain crystalline integrity at ambient temperature. The thermal stability of **1** was also explored by thermogravimetric (TG) and differential scanning calorimetric (DSC) analysis, as illustrated in Figure S4. The temperature for **1** exhibiting initial mass loss of 2.83% was 275 °C, assigned to the loss of corresponding solvent molecules (Calcd 3.79%). This was confirmed by DSC, since the spectrum exhibited an endothermic peak around 100 °C. With respect to **1**, the temperature at which **3** displayed an initial mass loss of 2.62% was 286 °C. This is attributable to loss of the corresponding methanol molecules (Calcd 2.26%) and is confirmed from DSC spectrum which exhibited an endothermic peak near 189.6 °C (Figure S5).

Luminescent compounds have received attention due to their applications as photoactive materials. Coordination architecture with group IIB metal centers and conjugated organic synthon may be candidates for potential fluorescent materials. The luminescence of conjugated organic compound can be altered by the subtle structural and environmental changes, especially for metal coordination. As depicted in Figure S6, free pbmb presents high-energy emission with a maximum of 384 nm ($\lambda_{\text{ex}} = 285$ nm), which could be attributed to the $\pi^*-\pi$

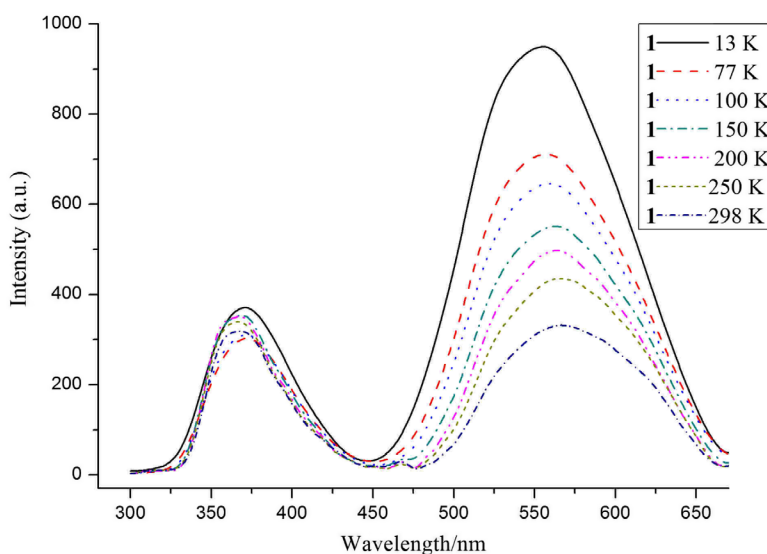


Figure 6. The luminescence curves of **1** upon excitation of 280 nm.

transitions [38]. The small Stokes shifts together with the nanosecond (ns) lifetime range are indicative of singlet state transitions (Table S1).

To explore luminescence thermochromic phenomena, the photoluminescence behavior of as-synthesized **1** was investigated at ambient and cryogenic temperatures to track its response (Figure 6). Complex **1** exhibited two emission bands with maxima at 370 and 562 nm. Upon cooling, the maximum emission peaks did not exhibit any obvious shift, whereas there was a relative increase in the intensity. Unlike pbmb, **1** gives weak high-energy bands ($\lambda_{\text{max}} = 375$ nm) with lifetimes in the ns range, where the lifetime τ is equal to 0.070 ± 0.002 ns at 298 K. In comparison with free pbmb, the reduced fluorescence lifetime of **1** may be ascribed to the coordinated Ag(I) center, which would increase the spin-orbit coupling and facilitate intersystem crossing from singlet to triplet excited states. Complex **1**, however, exhibits intense broad low-energy band emissions ($\lambda_{\text{max}} = 562$ nm) at 13, 77, 100, 150, 200, 250, and 298 K with corresponding lifetimes $\tau = 19.7 \pm 0.9$, 19 ± 1 , 19 ± 1 , 14.7 ± 0.4 , 12.6 ± 0.2 , 11.7 ± 0.2 , and 9.1 ± 0.2 ms, respectively. Together with the large Stokes shift, these emissions can be assigned to phosphorescence [39, 40]. The slight increase of triplet lifetime upon cooling may be caused by reduction of the nonradiative decay [41, 42].

The fluorescent properties of **2** and **3**, as well as pbmb, have been investigated in the solid-state at room temperature. The free pbmb shows an emission maximum at 379 nm upon excitation at either 279 nm or 343 nm. As depicted in Figure 7, **2** exhibits a maximum emission wavelength of 387 nm upon excitation at 279 nm resembling that of the free pbmb, which may be assigned to intraligand ($\pi-\pi^*$) charge transfer [43, 44]. Compared with pbmb, **2** exhibits significant fluorescence enhancement, which can be ascribed to chelating of the ligand to Cd, which increases the rigidity of the ligand and effectively reduces the loss of energy. Complex **2** has potential applications as a fluorescent material due to its excellent fluorescent properties. Moreover, different anions and coordination environments also have a certain effect on the luminescence behavior of complexes. As shown in Figure 8, the

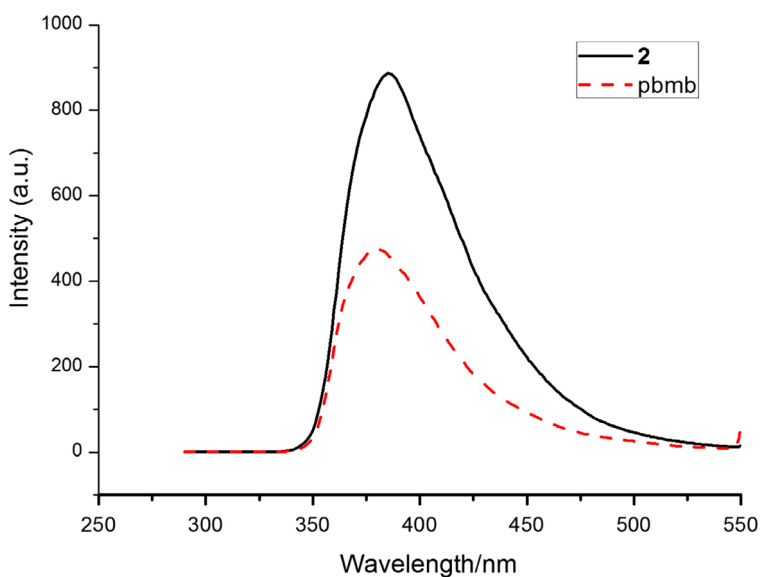


Figure 7. The luminescence curves of **2** and pbmb.

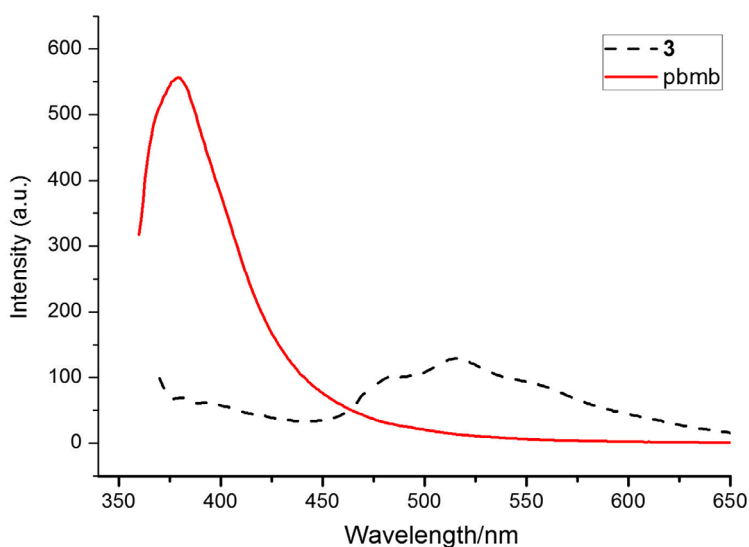


Figure 8. The luminescence curves of **3** and pbmb.

emission spectra of **3** exhibits two weak peaks at 381 and 516 nm with an excitation band at 343 nm. The Stokes shift of the emission band under low energy is 173 nm and 38 nm under high energy. Compared to the free ligand, the fluorescence intensity of **3** is extremely weak, which may be attributed to the heavy atom effect. The iodide coordinates effectively boosting the spin-orbit coupling and increasing the efficiency of the inter-system crossing from the singlet to the triplet excited state.

4. Conclusion

We synthesized three new complexes based on pbmb and they were characterized using single-crystal X-ray diffraction. Crystal structure analysis revealed that **1** and **2** feature 1-D chains, while **3** exhibited a tetranuclear structure. The photoluminescence study indicated that **2** has strong fluorescence intensity, and therefore, can be used as a luminescent material. On account of the heavy atom effect, **1** and **3** weaken the fluorescence intensities, which increase the spin-orbit coupling and the efficiency of the inter-system crossing. It can be observed that the heavy atom effect has a causative influence on the complexes, and their luminescent properties can be affected by different metal centers and anions.

Supplementary material

Crystallographic data for the structural analysis have been deposited with the Cambridge Crystallographic Data Center, CCDC reference numbers 1038939, 1563528, and 1563529. These data can be obtained free of charge via www.ccdc.cam.ac.uk/conts/retrieving.htm (or from the Cambridge Crystallographic Data Center, 12 Union Road, Cambridge CB2 1EZ, UK; Fax:+44 1223 336033).

Disclosure statement

No potential conflict of interest was reported by the authors.

Funding

This work was financially support by the National Natural Science Foundation of China [grant number 21401041] and the funding program for Academic technology leaders of He'nan University of Urban Construction [grant number YCJXSJSDTR201705].

References

- [1] M.J.S. Fard, N. Ghanbari, F. Rastaghi. *Inorg. Chim. Acta*, **396**, 149 (2013).
- [2] M.-P. Santoni, G.S. Hanan, B. Hasenknopf. *Coord. Chem. Rev.*, **281**, 64 (2014).
- [3] Z. Ma, B. Moulton. *Coord. Chem. Rev.*, **255**, 1623 (2011).
- [4] S. Gomez-Coca, E. Cremades, N. Aliaga-Alcalde, E. Ruiz. *J. Am. Chem. Soc.*, **135**, 7010 (2013).
- [5] S.-Z. Zhan, M. Li, X.-P. Zhou, J. Ni, X.-C. Huang, D. Li. *Inorg. Chem.*, **50**, 8879 (2011).
- [6] I. Bassanetti, F. Mezzadri, A. Comotti, P. Sozzani, M. Gennari, G. Calestani, L. Marchiò. *J. Am. Chem. Soc.*, **134**, 9142 (2012).
- [7] Q.-L. Zhang, Y.-L. Huang, H. Xu, B. Tu, B.-X. Zhu. *J. Coord. Chem.*, **70**, 156 (2017).
- [8] W. Cheng, T. Wang, W. Xu, Y. Zhang, J. Zhang, M. Fang. *J. Coord. Chem.*, **69**, 2220 (2016).
- [9] Q. Zhang, G. Feng, Y. Zhang, B. Zhu, L.F. Lindoy, G. Wei. *J. Coord. Chem.*, **69**, 253 (2016).
- [10] J.-H. Wang, G.-M. Tang, T.-X. Qin, Y.-T. Wang, Y.-Z. Cui, S.W. Ng. *J. Coord. Chem.*, **70**, 1168 (2017).
- [11] Y.-J. Li, Y.-L. Wang, W.-Y. Xu, C.-B. Han, Q.-Y. Liu. *J. Coord. Chem.*, **70**, 127 (2017).
- [12] Y.-G. Sun, S.-F. Ji, P. Huo, J.-X. Yin, Y.-D. Huang, Q.-Y. Zhu. *Inorg. Chem.*, **53**, 3078 (2014).
- [13] J. Eberhard, I. Stoll, R. Brockhinke, B. Neumann, H.-G. Stammer, A. Riefer, E. Rauls, W.G. Schmidt, J. Mattay. *CrystEngComm*, **15**, 4225 (2013).
- [14] S. Sculfort, P. Braunstein. *Chem. Soc. Rev.*, **40**, 2741 (2011).
- [15] Y.-P. Xie, T.C.W. Mak. *J. Am. Chem. Soc.*, **133**, 3760 (2011).
- [16] C. Wang, H.-Y. Li, G.-L. Guo, P. Wang. *Transition Met. Chem.*, **38**, 275 (2013).
- [17] J. Hu, C. Liao, S. Chen, P. Jin, J. Zhao, H. Zhao. *Inorg. Chem. Commun.*, **43**, 126 (2014).
- [18] X. Cheng, T. Liu, X. Duan, F. Wang, Q. Meng, C. Lu. *CrystEngComm*, **13**, 1314 (2011).
- [19] J. Zheng, Y.-D. Yu, F.-F. Liu, B.-Y. Liu, G. Wei, X.-C. Huang. *Chem. Commun.*, **50**, 9000 (2014).

- [20] A. Castineiras, N. Fernandez-Hermida, I. Garcia-Santos, J.L. Perez-Lustres, I. Rodriguez-Gonzalez. *Dalton Trans.*, **41**, 3787 (2012).
- [21] Y. Zhou, X. Zhang, W. Chen, H. Qiu. *J. Organomet. Chem.*, **693**, 205 (2008).
- [22] O.V. Dolomanov, L.J. Bourhis, R.J. Gildea, J.A.K. Howard, H. Puschmann. *J. Appl. Cryst.*, **42**, 339 (2009).
- [23] L. Palatinus, G. Chapuis. *J. Appl. Cryst.*, **40**, 786 (2007).
- [24] L. Palatinus, A. van der Lee. *J. Appl. Cryst.*, **41**, 975 (2008).
- [25] L. Palatinus, S.J. Prathapa, S. van Smaalen. *J. Appl. Cryst.*, **45**, 575 (2012).
- [26] G.M. Sheldrick. *Acta Cryst.*, **C71**, 3 (2015).
- [27] X.-Z. Song, C. Qin, W. Guan, S.-Y. Song, H.-J. Zhang. *New J. Chem.*, **36**, 877 (2012).
- [28] Y. Cui, C. He. *J. Am. Chem. Soc.*, **125**, 16202 (2003).
- [29] C.-F. Yan, Y.-X. Lin, F.-L. Jiang, M.-C. Hong. *Inorg. Chem. Commun.*, **43**, 19 (2014).
- [30] J. Pan, F.-L. Jiang, M.-Y. Wu, L. Chen, Y.-L. Gai, S.M. Bawaked, M. Mokhtar, S. A. AL-Thabaiti, M.-C. Hong. *Cryst. Growth Des.*, **14**, 5011 (2014).
- [31] C. Pettinari, J. Ngoune, A. Marinelli, B.W. Skelton, A.H. White. *Inorg. Chim. Acta*, **362**, 3225 (2009).
- [32] C.-W. Yeh, T.-R. Chen, J.-D. Chen, J.-C. Wang. *Cryst. Growth Des.*, **9**, 2595 (2009).
- [33] L. Qin, K. Lu, Z.-Y. Zheng, D.-T. Lin, J.-J. Zhao, D.-Y. Ma, F.-L. Liang. *J. Coord. Chem.*, **69**, 2210 (2016).
- [34] C. Xu, L. Li, Y. Wang, Q. Guo, X. Wang, H. Hou, Y. Fan. *Cryst. Growth Des.*, **11**, 4667 (2011).
- [35] C.-B. Fan, X.-M. Meng, Y.-H. Fan, L.-S. Cui, X. Zhang, C.-F. Bi. *J. Coord. Chem.*, **70**, 734 (2017).
- [36] C. Sen, A. Nandi, D. Mallick, S. Mondal, K.K. Sarker, C. Sinha. *Spectrochim. Acta, Part A*, **137**, 935 (2015).
- [37] C.-J. Li, S.-R. Zheng, Z.-Y. Chen, W.-D. Hu, S.-L. Cai, J. Fan, W.-G. Zhang. *J. Coord. Chem.*, **70**, 135 (2017).
- [38] H.-F. Ma, L.-W. Ding, L. Chen, Y.-L. Wang, Q.-Y. Liu. *J. Coord. Chem.*, **70**, 145 (2017).
- [39] C.-Q. Wan, T.C.W. Mak. *Cryst. Growth Des.*, **11**, 832 (2011).
- [40] V.K.-M. Au, D.P.-K. Tsang, K.M.-C. Wong, M.-Y. Chan, N. Zhu, V.W.-W. Yam. *Inorg. Chem.*, **52**, 12713 (2013).
- [41] J. Hu, J. Zhang, J. Zhao, L. Hu, S. Chen. *J. Coord. Chem.*, **69**, 574 (2016).
- [42] K. Kirakci, K. Fejfarová, J. Martinčík, M. Nikl, K. Lang. *Inorg. Chem.*, **56**, 4609 (2017).
- [43] E.M. Njogu, B. Omondi, V.O. Nyamori. *J. Coord. Chem.*, **70**, 2796 (2017).
- [44] T.S. Sukhikh, D.S. Ogienko, D.A. Bashirov, N.V. Kuratieva, V.Y. Komarov, M.I. Rakhmanova, S.N. Konchenko. *J. Coord. Chem.*, **69**, 3284 (2016).

Copyright of Journal of Coordination Chemistry is the property of Taylor & Francis Ltd and its content may not be copied or emailed to multiple sites or posted to a listserv without the copyright holder's express written permission. However, users may print, download, or email articles for individual use.